DOI: 10.1002/ejic.200800232

Crystal Structures and Magnetic Behaviors of Cyanido-Bridged Dinuclear Dimetallic Systems Involving 3d–3d or 3d–5d Metal Centers

Jae Il Kim,[a] Jung Hee Yoon,[a] Hyun Young Kwak,[a] Eui Kwan Koh,[b] and Chang Seop Hong*[a]

Keywords: Magnetism / Crystal structure / Cyanides / Dinuclear complexes / N ligands

Three cyanido-bridged Fe^{III}–Mn^{II} dimers, $[Fe(pzcq)(CN)_3][Mn(phen)_2(X)]\cdot MeOH$ [X = Cl (**1**), Br (**2**); pzcq = 8-(pyrazine-2-carboxamido)quinoline anion, phen = 1,10-phenanthroline], $[Fe(mpzcq)(CN)_3][Mn(phen)_2(Cl)]\cdot MeOH$ [**3**; mpzcq = 8-(5-methylpyrazine-2-carboxamido)quinoline anion], and one W^{V}–Mn^{II} dinuclear system, $[W(bpy)(CN)_6][Mn(phen)_2(Cl)]\cdot MeOH$ (**4**; bpy = 2,2′-bipyridine), were prepared by assembling molecular precursors, $[Fe(pzcq)(CN)_3]^-$, $[Fe(mpzcq)(CN)_3]^-$, and $[W(bpy)(CN)_6]^-$, with $Mn(phen)_2X_2$. The absolute configurations of the Mn polyhedra surrounded by two bidentate phen ligands are packed in a –Δ–Λ–Δ–Λ– sequence in the crystal lattice. The aromatic rings of the coordinated phen ligands are sources of considerable interdimer π–π contacts, which eventually lead to the formation of two-dimensional frameworks (**1**–**3**) and a one-dimensional chain structure (**4**). Magnetic analyses of the Fe^{III}–Mn^{II} dinuclear systems (**1**–**3**) reveal that a shorter Mn–N(cyanide) bond and a more linear Mn–N–C(cyanide) angle allow for stronger magnetic exchange coupling. Moreover, it is manifested that the 3d–5d magnetic coupling in **4** is stronger than the 3d–3d coupling in **1**–**3** under the given structural environments, which is due to the fact that the 5d orbital is more diffuse than the 3d orbital.

Introduction

In recent years, intensive attention has been paid to cyanido-bridged magnetic materials because of their underlying merits, such as relatively strong magnetic exchange coupling with predictable magnetic nature and photoresponsive properties upon irradiation. Cyanidometalates $[A(CN)_6]^{m-}$ (A = V, Cr, Mn, Fe), $[Mo(CN)_7]^{4-}$, and $[B(CN)_8]^{n-}$ (B = Mo, W, Nb, Re) have been successfully applied as molecular building blocks to the construction of intriguing molecule-based magnetic systems.[1–3] Self-assembly of the anionic motifs with paramagnetic metal cations decorated by chelating groups produced discrete molecules and multidimensional coordination polymers exhibiting slow magnetic relaxation,[4] high T_C values,[5] photomagnetic character,[6] and magnetic properties combined with chirality.[7] For instance, cyanido-linked dimetallic clusters, $\{M[M(Sol)_3]_8[M'(CN)_8]_6\}\cdot x Sol\cdot y H_2O$ (M = Mn, Co, Ni; M′ = Mo, W; Sol = MeOH or EtOH), which are able to be structurally modified, were found to display high ground-state spins of up to $S = 39/2$, and some of them exhibited slow magnetization relaxation.[8]

A sensible approach to generate dimensionally restricted assemblies, which are required to study the correct magnetic coupling and independent anisotropic nature of these systems, is the utilization of capped molecular entities, $[ML_p(CN)_q]^{n-}$ (M = paramagnetic metal ions, L = polydentate ligands), whose blocking groups can serve to preclude a structural extension in all directions.[9] A limited number of such molecular synthons have been developed, and among them low-spin Fe^{III} complexes have been most recognized as one of the sources of magnetic anisotropy. A variety of newly prepared Fe^{III} precursors emerged whose properties are dependent on the denticity of existing ligands, and these were used to design molecule-based objects with desirable features. They are, for example, $[Fe(L1)(CN)_5]^{2-}$ [L1 = monodentate nitrogen donor: 1-methylimidazole],[10] $[Fe(L2)(CN)_4]^-$ [L2 = bidentate nitrogen donor: bpy, phen, 2,2′-bipyrimidine (bpym)],[11] *fac*-$[Fe(L3)(CN)_3]^-$ [L3 = facially coordinated tridentate nitrogen donor: hydridotris(pyrazolyl)borate (Tp), hydridotris(3,5-dimethylpyrazol-1-yl)borate (Tp*), tetra(pyrazol-1-yl)borate (pzTp), 1,3,5-triaminocyclohexane (tach)],[12] *mer*-$[Fe(L4)(CN)_3]^-$ (L4 = meridionally coordinated tridentate nitrogen donor: bis(2-pyridylcarbonyl)amidate anion (bpca), 8-(pyridine-2-carboxamido)quinoline anion (pcq), pzcq, mpzcq],[13] and $[Fe(L5)(CN)_2]^-$ [L5 = tetradentate nitrogen donor: 1,2-bis(pyridine-2-carboxamido)benzenate (bpb)].[14]

[a] Department of Chemistry and Center for Electro- and Photo-Responsive Molecules, Korea University,
Seoul 136-713, Korea
E-mail: cshong@korea.ac.kr
[b] Nano-Bio System Research Team, Korea Basic Science Institute,
Seoul 136-713, Korea

Supporting information for this article is available on the WWW under http://www.eurjic.org or from the author.

Besides, subsequent advances in the fabrication of new 4d/5d precursors opened an opportunity to strengthen the magnetic coupling between corresponding spin carriers. To the best of our knowledge, only three molecular units, $[M(L)(CN)_3]^{n-}$ (M = Mo^{III}, Re^{II}; L = tridentate ligand) and octacoordinated $[W(bpy)(CN)_6]^-$, have been reported to date.[15] The molecular building blocks underwent reactions with appropriate paramagnetic moieties to afford single-molecule magnets and zigzag chain structures with spin-canting and metamagnetic characters.[15]

From a magnetic point of view, specific magnetic complexes with unique coordination geometries need to be investigated in the search for an understanding of the general magnetic exchange mechanism applicable to related systems.[16,17] As a matter of fact, to establish a magnetostructural correlation occurring in a family of compounds of interest containing cyanido bridges, it is reasonable to devise a simple model system that solely possesses one available magnetic pathway. In this regard, one of the judicial strategies is to invent a series of dinuclear complexes (one-*J* systems) with systematic structural variations, because trinuclear clusters or clusters of higher nuclearity frequently have different bond lengths and angles subject to magnetic pathways, which would lead to more than two magnetic routes.[10–14] To do this, the proper selection of precursors and their counterparts would still be a challenge.

Herein we present the syntheses, crystal structures, and magnetic properties of three cyanido-bridged Fe^{III}–Mn^{II} dimers, $[Fe(pzcq)(CN)_3][Mn(phen)_2(X)]\cdot MeOH$ [X = Cl (**1**), Br (**2**)], $[Fe(mpzcq)(CN)_3][Mn(phen)_2(Cl)]\cdot MeOH$ (**3**), and one W^{V}–Mn^{II} dinuclear complex, $[W(bpy)(CN)_6][Mn(phen)_2(Cl)]\cdot MeOH$ (**4**). The attempted modulation of ligand size and bulkiness, as well as metal ion in this case, brings about the subtle alteration of structural data related to the cyanido bridges. The extensive intermolecular π–π stackings between planar phen ligands account for the formation of two-dimensional networks (**1**–**3**) and a one-dimensional chain (**4**) in the lattice. Magnetic measurements for the dinuclear systems point out that the structural parameters in the bridging pathways as well as the metal constituents are responsible for the magnitude of the magnetic exchange coupling constants.

Results and Discussion

Synthesis and Characterization

The dinuclear Fe–Mn and W–Mn complexes (**1**–**4**) were isolated in spite of the reaction ratio of Fe(W)/Mn of 2:1, which indicates the stability of the products in the present experimental conditions. This is partly because $Mn(phen)_2X_2$ (X = Cl, Br) cannot accommodate two bulky Fe(W) moieties in a *cis* mode at the same time. In the IR spectra, the peculiar C≡N stretching vibrations of **1** are visible at 2141 (w) and 2124 (m) cm^{-1}, and those of **2** at 2158 (m), 2141 (m), 2123 (m), and 2112 (m, sh) cm^{-1}; these are shifted to higher frequencies relative to the reference cyanido peaks at 2123 (m) cm^{-1} for $K[Fe(pzcq)(CN)_3]$ and 2114 cm^{-1} for $(PPh_4)[Fe(pzcq)(CN)_3]$. For **3**, the cyanido peaks are observed at 2137 (m) and 2125 (m) cm^{-1}, and these are also positioned at higher frequencies with reference to the peaks at 2121 (m) and 2114 (m) cm^{-1} for $K[Fe(mpzcq)(CN)_3]$ and 2127 (m) and 2114 (m) cm^{-1} for $(PPh_4)[Fe(mpzcq)(CN)_3]$. The C≡N bands of **4** are present at 2179 (m), 2150 (w), 2135 (w, sh), and 2133 (w) cm^{-1}, whereas the W precursor has peaks at 2160 (m), 2151 (w), 2144 (w), 2134 (w), and 2124 (w) cm^{-1}. The IR data thus provide concurrent evidence for the existence of terminal and bridging cyanido ligands. The shift of cyanido peaks toward higher frequencies is pertinent to the prevalent kinematic effect, which leads to the restriction of the motion of the cyanido ligands, as well as electronic and geometric effects.[18]

Description of the Structures

Compounds **1**–**3** are shown in Figure 1 with selected atom-labelling schemes. Selected bond lengths and angles are summarized in Table 1. Each Fe center adopts a distorted octahedral geometry consisting of three C atoms from terminal cyanido ligands and three N atoms from the tridentate ligand. The Fe–C(cyanide) bond lengths are in the ranges of 1.944–1.954 Å for **1**, 1.945–1.966 Å for **2**, and 1.941–1.977 Å for **3**. The Fe–N(amide) bond lengths are shorter [1.873(3) Å for **1**, 1.882(3) Å for **2**, and 1.879(3) Å for **3**] than those of the other Fe–N bonds which span from 1.946 to 1.975 Å and are due to the strong σ-donor effect of the deprotonated amide.[13] The Fe–C–N angles are almost linear, with the maximum deviations from linearity being 4.5° for **1**, 5.6° for **2**, and 4.3° for **3**. In **4** (Figure 2), the W1 center is octahedrally coordinated by four C atoms from CN groups and two N atoms from bpy [W–C_{av} 2.15(1) Å, W–N_{av} 2.2160(3) Å]. The exact geometry of the W atom can be determined by means of a continuous shape measure (CShM) analysis (Table 2).[19] The S_X (X = SAPR, DD, BTP) value against the ideal symmetries for a square antiprism (SAPR, D_{4d}), a dodecahedron (DD, D_{2d}), and a bicapped trigonal prism (BTP, C_{2v}) corresponds to zero when the polyhedral shape is identical to the reference geometry and deviates from zero when the analyzed polyhedron is distorted.[20] The obtained S_X values for the W1 environment indicate that the geometry of W1 is close to that of an SAPR. The small Δ value shows that the actual shape is in the interconversion path between an SAPR and a DD. Eventually, the CShM analysis clearly reveals that W1 takes on a distorted SAPR arrangement.

The geometry around an Mn ion can be described as that of a distorted octahedron made up of four N atoms from two phen ligands, one Cl or Br atom, and one N atom from a bridging cyanido ligand. The average Mn–N(phen) bond lengths are much alike: 2.29(2) Å for **1**, 2.29(3) Å for **2**, 2.30(2) Å for **3**, and 2.29(2) Å for **4**. The Mn–Cl lengths in **1**, **3**, and **4** are also similar and are in the range of 2.4342–2.4368 Å, whereas **2** exhibits an Mn–Br length of 2.6124(8) Å. For **1** and **2**, the coordination of the bulkier Br group to the Mn center rather than the Cl atom affects

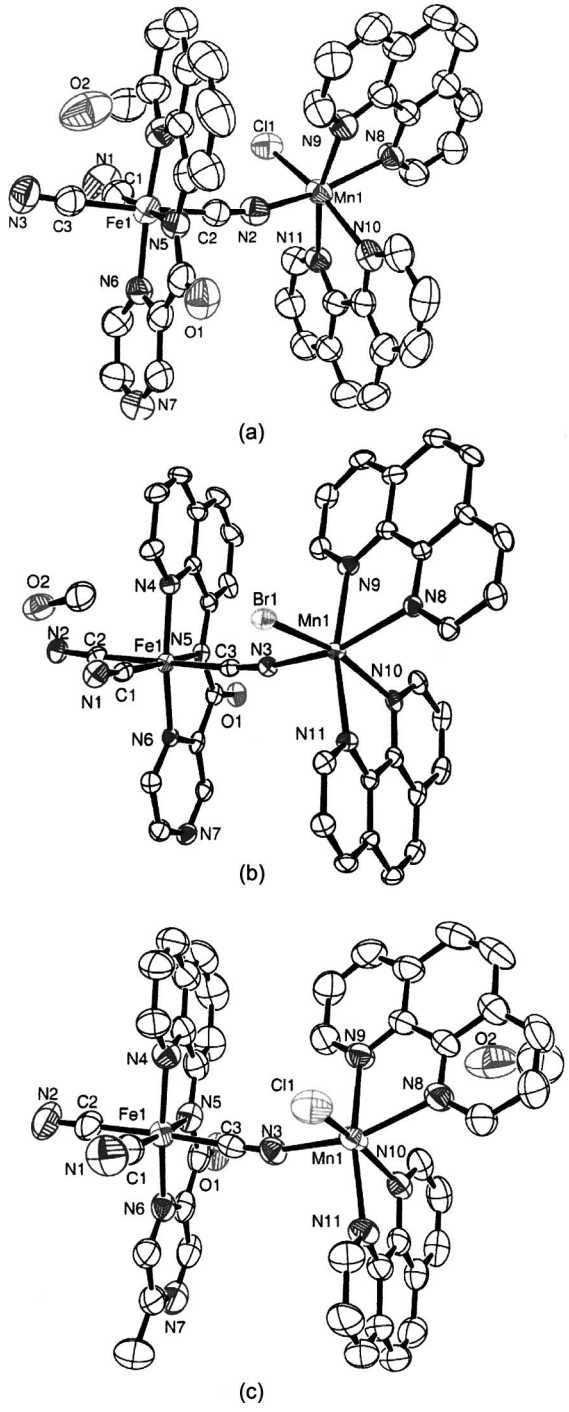

Figure 1. ORTEP diagrams of (a) **1**, (b) **2**, and (c) **3** with selected atom-labelling schemes.

Table 1. Selected bond lengths [Å] and angles [°] for **1**–**4**.

Compound **1**			
Fe(1)–N(5)	1.873(3)	Fe(1)–C(1)	1.944(5)
Fe(1)–C(3)	1.945(5)	Fe(1)–N(4)	1.946(4)
Fe(1)–C(2)	1.954(5)	Fe(1)–N(6)	1.975(4)
N(2)–Mn(1)	2.210(4)	Mn(1)–N(8)	2.265(4)
Mn(1)–N(11)	2.282(4)	Mn(1)–N(10)	2.289(4)
Mn(1)–N(9)	2.313(4)	Mn(1)–Cl(1)	2.4368(14)
N(1)–C(1)–Fe(1)	176.3(5)	N(2)–C(2)–Fe(1)	175.5(4)
C(2)–N(2)–Mn(1)	167.5(4)	N(3)–C(3)–Fe(1)	178.8(5)
Compound **2**			
Fe(1)–N(5)	1.882(3)	Fe(1)–C(2)	1.945(5)
Fe(1)–C(1)	1.949(4)	Fe(1)–N(4)	1.962(3)
Fe(1)–N(6)	1.964(3)	Fe(1)–C(3)	1.966(4)
N(3)–Mn(1)	2.200(4)	Mn(1)–N(8)	2.259(3)
Mn(1)–N(10)	2.282(3)	Mn(1)–N(11)	2.290(3)
Mn(1)–N(9)	2.322(3)	Mn(1)–Br(1)	2.6134(8)
N(1)–C(1)–Fe(1)	175.7(4)	N(2)–C(2)–Fe(1)	178.0(4)
N(3)–C(3)–Fe(1)	174.4(4)	C(3)–N(3)–Mn(1)	169.2(3)
Compound **3**			
Fe(1)–N(5)	1.879(3)	Fe(1)–C(2)	1.941(4)
Fe(1)–C(1)	1.947(4)	Fe(1)–N(4)	1.969(3)
Fe(1)–N(6)	1.974(3)	Fe(1)–C(3)	1.977(4)
N(3)–Mn(1)	2.220(3)	Mn(1)–N(8)	2.280(3)
Mn(1)–N(11)	2.282(3)	Mn(1)–N(10)	2.290(3)
Mn(1)–N(9)	2.332(3)	Mn(1)–Cl(1)	2.4342(11)
N(1)–C(1)–Fe(1)	175.7(4)	N(2)–C(2)–Fe(1)	179.5(3)
N(3)–C(3)–Fe(1)	177.5(3)	C(3)–N(3)–Mn(1)	165.8(3)
Compound **4**			
W(1)–C(4)	2.131(2)	W(1)–C(2)	2.149(2)
W(1)–C(1)	2.152(2)	W(1)–C(6)	2.157(3)
W(1)–C(5)	2.159(3)	W(1)–C(3)	2.172(2)
W(1)–N(8)	2.2158(18)	W(1)–N(7)	2.2162(18)
N(1)–Mn(1)	2.199(2)	Mn(1)–N(12)	2.258(2)
Mn(1)–N(10)	2.278(2)	Mn(1)–N(11)	2.291(2)
Mn(1)–N(9)	2.317(2)	Mn(1)–Cl(1)	2.4363(7)
N(6)–C(6)–W(1)	177.6(3)	N(5)–C(5)–W(1)	177.7(2)
N(2)–C(2)–W(1)	176.6(2)	N(3)–C(3)–W(1)	177.1(2)
N(4)–C(4)–W(1)	179.9(3)	N(1)–C(1)–W(1)	177.4(2)
C(1)–N(1)–Mn(1)	163.8(2)		

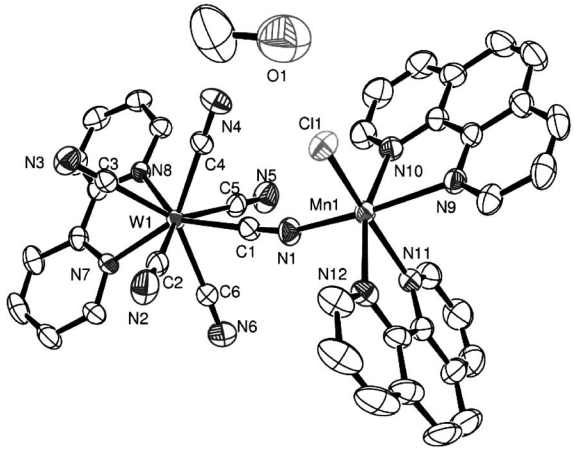

Figure 2. ORTEP diagram of **4** with selected atom-labelling scheme.

adjoining structural parameters. The Mn–N(cyanide) bond [Mn1–N3 2.200(4) Å] and the Mn–N–C(cyanide) angle (Mn1–N3–C3 169.2°) in **2** are shorter and larger than the corresponding parameters in **1** [Mn1–N2 2.210(4) Å, Mn1–N2–C2 167.5°], respectively. In the comparison of **3** with **1**, the presence of the methyl group in the chelating mpzcq ligand also changes the internal structure, as revealed by the longer Mn–N(cyanide) bond of 2.220(3) Å and the more acute Mn–N–C(cyanide) angle of 165.8°. In the case of **4**, the specific bond length [2.200(5) Å for Mn1–N1] is equal to that of **2** but is smaller than those of **1** and **3**. The angle [163.1(5)° for Mn1–N1–C1] in **4** is the smallest among

Table 2. Results of the continuous shape measure analysis.[a]

Metal center	S_{SAPR}	S_{DD}	S_{BTP}	$\Delta_{(SAPR, DD)}$	$\phi_{(SAPR > DD)}$	$\phi_{(DD > SAPR)}$
W1 in **4**	0.51	1.86	1.97	0.23	42%	81%

[a] S_{DD} is the shape measure relative to the dodecahedron, S_{SAPR} the shape measure relative to the square antiprism, and S_{BTP} the shape measure relative to the bicapped trigonal prism. $\Delta_{(SAPR, DD)}$ indicates the deviation from the DD–SAPR interconversion pathway, and $\phi_{(SAPR > DD)}$ and $\phi_{(DD > SAPR)}$ the generalized interconversion coordinates. The sum $\phi_{(SAPR > DD)} + \phi_{(DD > SAPR)}$ is larger than 100% because of the nonzero value of $\Delta_{(SAPR, DD)}$.

all the complexes. The intradimer Fe(W)–Mn distances are 2.2673(14) Å for **1**, 5.2732(9) Å for **2**, 5.2827(8) Å for **3**, and 5.4254(4) Å for **4**. The absolute configurations of the Mn octahedra in the asymmetric units, as depicted in Figures 1 and 2, are Δ for **1**, Λ for **2**, Λ for **3**, and Λ for **4**.

The extended views of **1** and **2** are isostructural to each other and a representative structure of **1** is illustrated in Figure 3. A one-dimensional supramolecular chain is formed by incorporating type I π–π stackings, which occur between the entire overlap of two adjacent pyridyl groups in the range of 3.474–3.508 Å for **1** and 3.442–3.468 Å for **2**, and type II intermolecular forces, which cause contacts between two sets of four aromatic C atoms (3.510–3.513 Å for **1** and 3.496–3.510 Å for **2**). The chirality of each Mn center in the chain fluctuates regularly in a –Λ–Δ–Λ–Δ– sequence and in turn becomes racemic in the crystal lattice. One-dimensional chains are interconnected through type III π–π interactions (3.446–3.447 Å for **1** and 3.393–3.411 Å for **2**), which finally leads to the construction of a two-dimensional network structure. For **3** (Figure 4), the configurations around the Mn ions designate a racemic –Δ–Λ–Δ–Λ– pattern throughout a chain formed by extensive noncovalent intermolecular type I (3.492–3.520 Å) and type II contacts (3.481–3.506 Å). A two-dimensional framework is provided by linking the chains together through type III stackings (3.713–3.716 Å). All of the π–π contacts found in **3** arise from interactions among sets of four aromatic C atoms of the phen ligands. The interdimer Mn–Mn distances across type I, type II, and type III interactions are 8.429, 9.154, and 10.394 Å for **1**; 8.361, 9.325, and 9.983 Å for **2**; and 9.352, 10.837, and 12.240 Å for **3**; respectively. Unlike **1**–**3**, compound **4** retains only two types of π–π forces to generate a one-dimensional chain in an alternat-

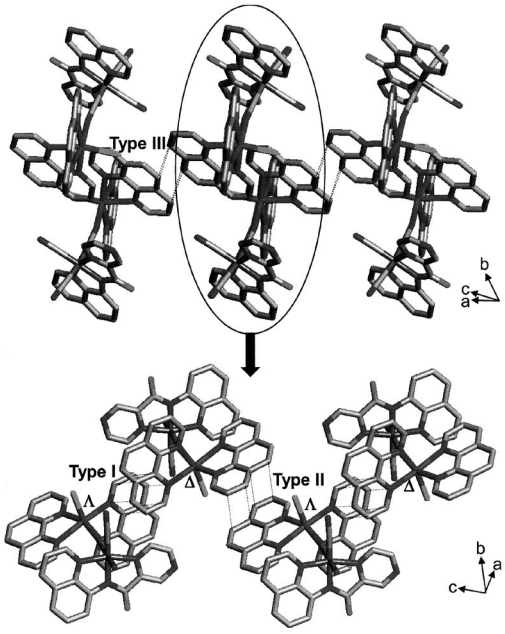

Figure 3. Extended structures of **1** showing the absolute configurations around the Mn centers and the intermolecular π–π contacts. The dotted lines represent the π–π stackings.

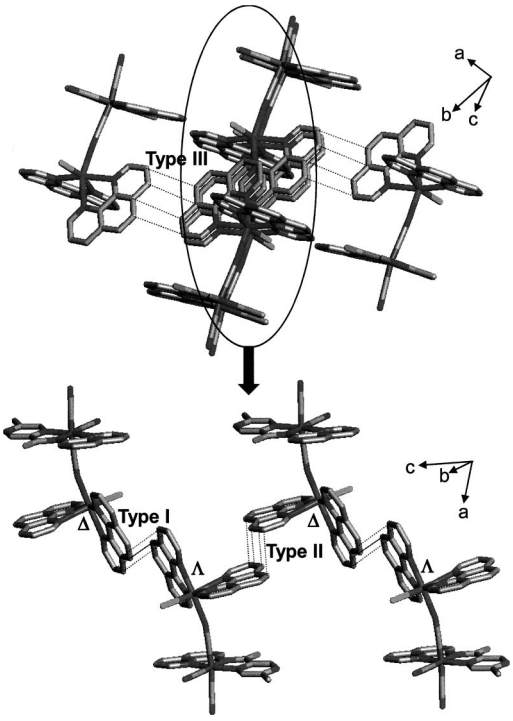

Figure 4. Extended structures of **3** showing the absolute configurations around the Mn centers and the intermolecular π–π interactions. The dotted lines represent the π–π contacts.

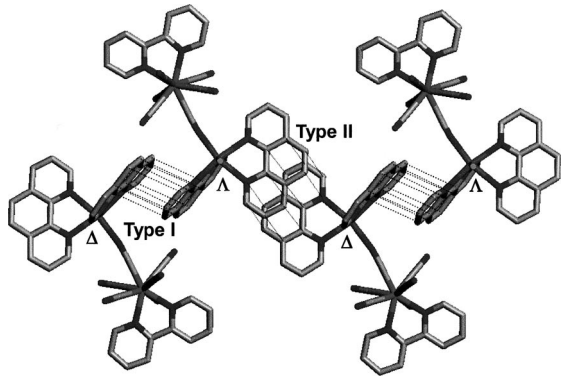

Figure 5. Extended structure of **4** showing the absolute configurations around the Mn centers and the intermolecular π–π interactions. The dotted lines represent the π–π contacts.

ing –Δ–Λ–Δ–Λ– pattern (Figure 5). Notably, the contact faces are more extensive than in **1**–**3** because the type I and type II contacts in **4** are composed of interactions between the quinoline subunits of the phen ligands. The interactions range from 3.556 to 3.709 Å for type I contacts and from 3.732 to 3.872 Å for type II contacts. The intermolecular Mn–Mn separations in **4** are 9.379 Å and 9.809 Å through type I and type II interactions, respectively. Hydrogen bonds are established between the O atoms of lattice MeOH molecules and the N atoms of unbound cyanido ligands [O2–N1 2.824(9) Å for **1**, 2.819(6) Å for **2**, 2.853(7) Å for **3**, and O1–N6 2.926(5) Å for **4**].

Magnetic Properties

The temperature dependences of the magnetic susceptibilities for **1**–**3** are shown in Figures 6, 7, and 8. The $\chi_m T$ values at 300 K are 4.80 (**1**), 4.79 (**2**), and 4.62 (**3**) $cm^3 K mol^{-1}$, which are close to the spin-only value (4.75 $cm^3 K mol^{-1}$) expected for one each of noninteracting Fe^{III} ($S_{Fe} = 1/2$) and Mn^{II} ($S_{Mn} = 5/2$) ions. As the temperature is lowered, $\chi_m T$ decreases gradually until 60 K, and below that temperature drops abruptly to 2.31 (**1**), 2.37 (**2**), and 2.49 (**3**) $cm^3 K mol^{-1}$ at 2 K. Noticeable shoulders in the $\chi_m T$ plots are visible at 3.19 (**1**), 2.98 (**2**), and 3.07 (**3**) $cm^3 K mol^{-1}$ at 8 K. The observed values are compatible with the theoretical one (3.00 $cm^3 K mol^{-1}$) calculated from $S = S_{Mn} - S_{Fe}$ with $g = 2$, which demonstrates that antiferromagnetic interactions between two spins within a dimer result in an $S = 2$ ground state. On the other hand, the W–Mn dimer **4** exhibits a magnetic trend resembling that of the Fe–Mn systems (Figure 9). The room-temperature $\chi_m T$ value is 4.66 $cm^3 K mol^{-1}$, which is consistent with those of **1**–**3**. A shoulder in the $\chi_m T$ curve is also observed at 3.07 $cm^3 K mol^{-1}$ at a temperature of 9 K, higher than that for **1**–**3** (8 K). The high-temperature data ($T > 15$ K) can be interpreted using the Curie–Weiss law [$\chi_m = C/(T - \theta)$], where C is the Curie constant and θ the Weiss constant. The obtained results are summarized in Table 3. The negative Weiss constants obviously support the existence of overall antiferromagnetic couplings among magnetic centers. It is noted that **3** shows the lowest value of θ, whereas **4** has the highest one, which may reflect the strength of the magnetic exchange interactions between the spin centers through the cyanido links. The field dependencies of the magnetization at 2 K (**1**–**3**) and 1.8 K (**4**) are shown in the insets of Figures 6, 7, 8, and 9. The magnetization data lie far below the theoretical curves based on one each of noncoupled Fe^{III} (or W^{V}) and Mn^{II} ions. This implies that there exist sizeable intradimer antiferromagnetic interactions. The experimental data are fairly well reproduced by the Brillouin curves derived from $S = S_{Mn} - S_{Fe(W)} = 2$.

To estimate the magnetic exchange coupling constants through the cyanido bridges, we employed the following equation derived from the isotropic spin Hamiltonian $H = -JS_1 \cdot S_2$ under consideration of the molecular field approximation (zJ'):[16]

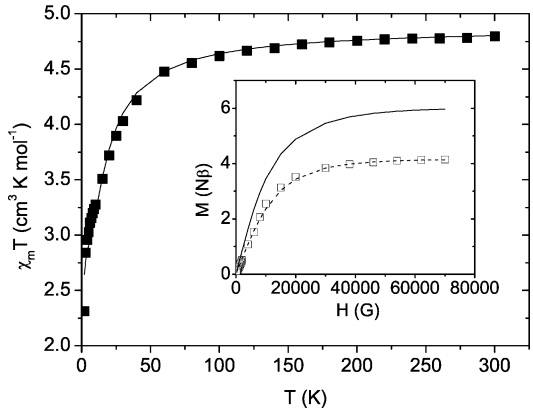

Figure 6. Plot of $\chi_m T$ vs. T for **1**. The solid line shows the best theoretical fit. The inset presents the field dependence of the magnetization per Fe–Mn at 2 K. The solid line denotes the Brillouin curve for one each of independent Fe^{III} and Mn^{II} ions, whereas the dashed line derives from the theoretical curve for $S = S_{Mn} - S_{Fe} = 2$.

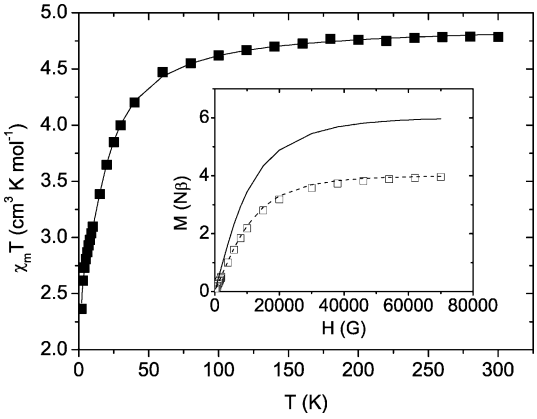

Figure 7. Plot of $\chi_m T$ vs. T for **2**. The solid line shows the best theoretical fit. The inset gives the field dependence of the magnetization per Fe–Mn at 2 K. The solid and dashed lines denote the Brillouin curves for one each of uncoupled Fe^{III} and Mn^{II} ions as well as for $S = S_{Mn} - S_{Fe} = 2$, respectively.

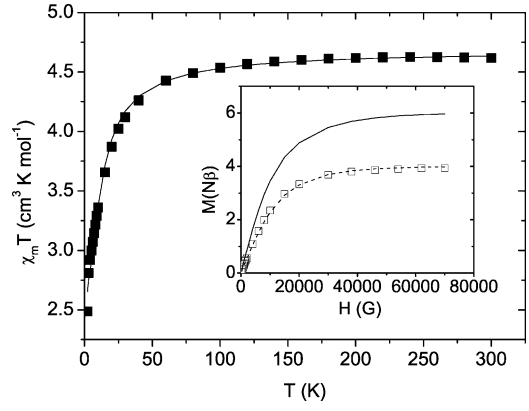

Figure 8. Plot of $\chi_m T$ vs. T for **3**. The solid line shows the best theoretical fit. The inset indicates the field dependence of the magnetization per Fe–Mn at 2 K. The solid line stands for the Brillouin curve for one each of independent Fe^{III} and Mn^{II} ions, whereas the dashed line comes from the theoretical curve for $S = S_{Mn} - S_{Fe} = 2$.

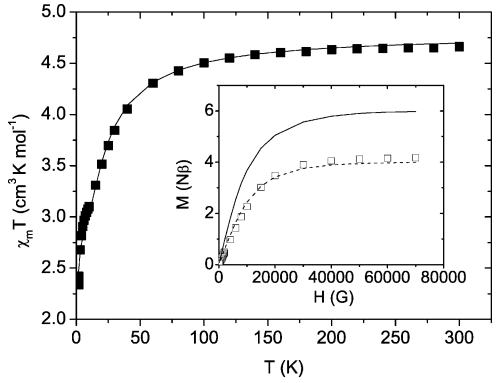

Figure 9. Plot of $\chi_m T$ vs. T for **4**. The solid line shows the best theoretical fit. The inset presents the field dependence of the magnetization per W–Mn at 1.8 K. The solid line stands for the Brillouin curve for one each of independent W^V and Mn^{II} ions, whereas the dashed line comes from the theoretical curve for $S = S_{Mn} - S_W = 2$.

Table 3. Magnetic data and fitted parameters for **1**–**4**.

	$\chi_m T$ at 300 K [$cm^3 K mol^{-1}$]	C [$cm^3 K mol^{-1}$]	θ [K]	J [cm^{-1}]
1	4.80	4.90	–6.1	–6.63
2	4.79	4.90	–6.4	–7.37
3	4.62	4.69	–3.7	–4.46
4	4.66	4.77	–6.6	–8.01

$$\chi_m = (2Ng^2\beta^2/kT)[5 + 14\exp(3J/kT)]/[5 + 7\exp(3J/kT)]$$

where J is the intradimer exchange coupling constant between spin centers. The least-squares fits give magnetic parameters of $g = 2.03$, $J = -6.63$ cm^{-1}, and $zJ' = -0.12$ cm^{-1} for **1**; $g = 2.03$, $J = -7.37$ cm^{-1}, and $zJ' = -0.20$ cm^{-1} for **2**; $g = 1.99$, $J = -4.46$ cm^{-1}, and $zJ' = -0.08$ cm^{-1} for **3**; and $g = 2.01$, $J = -8.01$ cm^{-1}, and $zJ' = -0.15$ cm^{-1} for **4**. The J values obtained for **1**–**4** are similar to those for the cyanido-linked Fe^{III}–Mn^{II} complexes[13b,14b,21] and octacyanidotungstate-based W^V–Mn^{II} clusters.[22] The negative J values undoubtedly suggest that antiferromagnetic interactions are truly operative through the cyanido bridges. The magnetic nature is a consequence of the sum of antiferromagnetic contributions from the π overlap between t_{2g} orbitals on Fe^{III} (t_{2g}^5 configuration) and t_{2g} orbitals on Mn^{II} ($t_{2g}^3e_g^2$ configuration) and ferromagnetic contributions from orthogonal orbitals [t_{2g}(Fe)–e_g(Mn) pairs].[16] Antiferromagnetic contributions dominate over the ferromagnetic pairs through the significant π overlap of d_{xz} and d_{yz} orbitals, if one assumes the z axis to be along the Fe–Mn axis, which may result in the observed antiferromagnetic arrangements in **1**–**3**.[16] On the basis of the magnetic feature in octacyanidometalate-based materials, one might conclude that the antiferromagnetic interactions in **4** are substantiated through the π pathway between the dπ orbitals on both metal ions.[23]

The current dinuclear systems with one-J magnetic pathways may provide more favorable examples by which to evaluate the precise exchange coupling between two specific spin centers, when compared with trinuclear or higher-nuclearity Fe^{III}–Mn^{II} clusters that often exhibit different bond lengths and angles and then possess more than two magnetic routes. We attempted to obtain a correlation between the J values and the structural parameters in the dimer series. For **1** and **2**, built by the same tricyanidoiron precursors and $Mn(phen)_2$ subunits with disparate halide ligands attached, the Mn–N(cyanide) bond length of 2.210(4) Å and Mn–N–C(cyanide) angle of 167.5(4)° for **1** are longer and smaller than the corresponding data [2.200(4) Å and 169.2(3)°] for **2**, respectively. These structural parameters affect the strength of the magnetic exchange, and as a result J is changed from –6.63 cm^{-1} (**1**) to –7.37 cm^{-1} (**2**). At the same time, this particular bond length and angle for **1** are shorter and more obtuse than those for **3** that comprise the precursor with the methyl substituent on the pyrazine ring. Such structural variations lead to the reduction of the J value to –4.46 cm^{-1} for **3**. From these observations, it appears that the magnetic strength is enhanced as the bond length becomes shorter and the angle more linear. The dependence of the magnetic exchange parameters on the special structural data is probably concerned to a degree with the efficient π overlap of the equivalent magnetic orbitals.[10,23] Furthermore, it is also interesting to inspect the magnetic nature of **4**, made of 5d and 3d metal ions, with respect to the other Fe^{III}–Mn^{II} dimers containing 3d and 3d metal ions. The Mn–N–C(cyanide) bond angle [163.8(2)°] of **4** marks the smallest among the present complexes, whereas the Mn–N(cyanide) bond length of **4** is almost identical to that of **2**. In view of the aforementioned relationship between the structural data and the J value, it is expected that the magnetic exchange strength of **4** is at least smaller than that of **2**. However, the reverse is true: **4** shows the strongest antiferromagnetic couplings among all of the complexes. Accordingly, a comparison of the magnetism between **4** and the others tentatively designates that 3d–5d magnetic coupling is stronger than 3d–3d coupling because the 5d valence orbital is spatially more expanded than the 3d orbital.[15c,20a] To determine the general trend in these systems, more related examples need to be prepared and studied.

Conclusions

We have prepared and characterized four cyanido-bridged dimetallic Fe^{III}–Mn^{II} and W^V–Mn^{II} dinuclear complexes. The Mn centers chelated with two bidentate phen ligands are arranged in a chiral –Δ–Λ–Δ–Λ– sequence in the crystal packing. The phen ligands participate in extensive intermolecular π–π interactions, which give rise to the fabrication of two-dimensional networks (**1**–**3**) and a one-dimensional chain system (**4**). The structural and magnetic analyses disclose that the length of the Mn–N(cyanide) bond and the bending of the Mn–N–C(cyanide) angle influence the strength of the magnetic exchange coupling between the two magnetic centers mediated by the cyanido bridges. The comparison of **1**–**3** with **4** tentatively demonstrates that 3d–5d magnetic coupling is stronger than 3d–

3d coupling under the given structural environments. Thus, the study of the dinuclear compounds provides a chance to gain insight into the magnetostructural relationship in the present system.

Experimental Section

Physical Measurements: Elemental analyses for C, H, and N were performed at the Elemental Analysis Service Center of Sogang University. IR spectra were obtained from KBr pellets with a Bomen MB-104 spectrometer. Magnetic susceptibilities for **1**–**4** were carried out using a Quantum Design MPMS-7 SQUID susceptometer at Seoul Branch, KBSI. Diamagnetic corrections for **1**–**4** were estimated from Pascal's constants.

Synthesis: $K[Fe(pzcq)(CN)_3]\cdot 2.5H_2O$,[13c] $(PPh_4)[Fe(mpzcq)(CN)_3]\cdot H_2O$,[13d] $(Ph_4As)[W(bpy)(CN)_6]$,[24] and $Mn(phen)_2Cl_2$[25] used in the synthesis were prepared according to literature procedures. All chemicals and solvents were of reagent grade and used as received. All manipulations were performed under aerobic conditions.

$[Fe(pzcq)(CN)_3][Mn(phen)_2(Cl)]\cdot MeOH$ (1): An MeOH (15 mL) solution of $Mn(phen)_2Cl_2$ (0.10 mmol) was slowly added to an MeCN (15 mL) solution of $K[Fe(pzcq)(CN)_3]\cdot 2.5H_2O$ (0.20 mmol). After stirring for a few minutes, the filtered solution was left undisturbed. Brown rod-shaped crystals suitable for X-ray analysis were obtained in a few days. Yield: 63%. $C_{42}H_{29}ClFeMnN_{11}O_2$ (866.00): calcd. C 58.25, H 3.38, N 17.79; found C 58.27, H 3.32, N 17.89.

$[Fe(pzcq)(CN)_3][Mn(phen)_2(Br)]\cdot MeOH$ (2): An MeOH (5 mL) solution of phen (0.20 mmol) was mixed with an MeOH (5 mL) solution of $MnBr_2$ (0.10 mmol). A solution of $K[Fe(pzcq)(CN)_3]\cdot 2.5H_2O$ (0.20 mmol) dissolved in MeOH/MeCN (1:1) was added dropwise with stirring to the resulting solution. Slow concentration of the filtered solution afforded brown crystals suitable for X-ray analysis. Yield: 56%. $C_{42}H_{29}BrFeMnN_{11}O_2$ (910.45): calcd. C 55.41, H 3.21, N 16.92; found C 55.87, H 3.19, N 16.65.

$[Fe(mpzcq)(CN)_3][Mn(phen)_2(Cl)]\cdot MeOH$ (3): A solution of $Mn(phen)_2Cl_2$ (0.025 mmol) in MeOH/MeCN (1:1) (10 mL) was slowly added to an MeCN (10 mL) solution of $(PPh_4)[Fe(mpzcq)(CN)_3]\cdot H_2O$ (0.050 mmol). The resultant solution was filtered after a few minutes of stirring and left undisturbed. Brown crystals formed in a few days. Yield: 56%. $C_{43}H_{31}ClFeMnN_{11}O_2$ (880.03): calcd. C 58.69, H 3.55, N 17.51; found C 58.34, H 3.59, N 17.43.

$[W(bpy)(CN)_6][Mn(phen)_2(Cl)]\cdot MeOH$ (4): An MeCN (10 mL) solution of $(Ph_4As)[W(bpy)(CN)_6]$ (0.045 mmol) was added to an MeOH (10 mL) solution of $Mn(phen)_2Cl_2$ (0.0225 mmol). Slow concentration of the filtered solution produced red crystals. Yield: 84%. $C_{41}H_{28}ClMnN_{12}OW$ (978.99): calcd. C 50.30, H 2.88, N 17.17; found C 50.59, H 2.94, N 17.75

Crystallographic Structure Determination: X-ray data for **1**–**4** were collected with a Bruker SMART APEXII diffractometer equipped with graphite-monochromated Mo-K_α radiation (λ = 0.71073 Å). Preliminary orientation matrix and cell parameters were determined from three sets of ω scans at different starting angles. Data frames were obtained at scan intervals of 0.5° with an exposure time of 10 s per frame. The reflection data were corrected for Lorentz and polarization factors. Absorption corrections were carried out using SADABS.[26] The structures were solved by direct methods and refined by full-matrix least-squares analysis using anisotropic thermal parameters for non-hydrogen atoms with the SHELXTL program.[27] All hydrogen atoms except for hydrogen atoms bound to MeOH molecules were calculated at idealized positions and refined with the riding models. Crystallographic data and details of data collection are provided in the Supporting Information (Table S1). CCDC-680086 (**1**), -680087 (**2**), -680088 (**3**), and -680089 (**4**) contain the supplementary crystallographic data for **1**–**4**. These data can be obtained free of charge from The Cambridge Crystallographic Data Centre via www.ccdc.cam.ac.uk/data_request/cif.

Supporting Information (see footnote on the first page of this article): Crystallographic data and details of the data collection for **1**–**4**.

Acknowledgments

This work was supported by Korea Research Foundation Grant (MOEHRD) (KRF-2006-331-C00158).

[1] a) D. Gimenez-Romero, J. Agrisuelas, J. J. Garcia-Jareno, J. Gregori, C. Gabrielli, H. Perrot, F. Vicente, *J. Am. Chem. Soc.* **2007**, *129*, 7121–7126; b) V. Marvaud, C. Decroix, A. Scuiller, F. Tuyeras, G.-C. Duhayon, J. Vaissermann, J. Marrot, F. Gonnet, M. Verdaguer, *Chem. Eur. J.* **2003**, *9*, 1692–1705; c) E. Colacio, M. Ghazi, H. Stoeckli-Evans, F. Lloret, J. M. Moreno, C. Perez, *Inorg. Chem.* **2001**, *40*, 4876–4883; d) M. Ohba, H. Okawa, *Coord. Chem. Rev.* **2000**, *198*, 313–328.

[2] a) J. Larionova, O. Kahn, J. Bartolome, R. Burriel, M. Castro, V. Ksenofontov, P. Gütlich, *Chem. Mater.* **1999**, *11*, 3400–3405; b) V. S. Mironov, L. F. Chibotaru, A. Ceulemans, *J. Am. Chem. Soc.* **2003**, *125*, 9750–9760.

[3] a) M. V. Bennett, J. R. Long, *J. Am. Chem. Soc.* **2003**, *125*, 2394–2395; b) R. Pradhan, C. Desplanches, P. Guionneau, J.-P. Sutter, *Inorg. Chem.* **2003**, *42*, 6607–6609; c) J. R. Withers, D. Li, T. Jeremy, C. Ruschman, S. Parkin, G. Wang, G. T. Yee, S. M. Holmes, *Polyhedron* **2007**, *26*, 2353–2366; d) D.-f. Li, S. Gao, L.-m. Zheng, W.-x. Tang, *J. Chem. Soc., Dalton Trans.* **2002**, 2805–2806; e) R. Podgajny, M. Balanda, M. Sikora, M. Borowiec, L. Spalek, C. Kapusta, B. Sieklucka, *Dalton Trans.* **2006**, 2801–2809; f) M. P. Shores, J. J. Sokol, J. R. Long, *J. Am. Chem. Soc.* **2002**, *124*, 2279–2292; g) E. Ruiz, A. Rodríguez-Fortea, S. Alvarez, M. Verdaguer, *Chem. Eur. J.* **2005**, *11*, 2135–2144.

[4] a) A. V. Palii, S. M. Ostrovsky, S. I. Klokishner, B. S. Tsukerblat, C. P. Berlinguette, K. R. Dunbar, J. R. Galán-Mascarós, *J. Am. Chem. Soc.* **2004**, *126*, 16860–16867; b) C. P. Berlinguette, D. Vaughn, C. Cañada-Vilalta, J. R. Galán-Mascarós, K. R. Dunbar, *Angew. Chem. Int. Ed.* **2003**, *42*, 1523–1526; c) M. Ferbinteanu, H. Miyasaka, W. Wernsdorfer, K. Nakata, K.-i. Sugiura, M. Yamashita, C. Coulon, R. Clérac, *J. Am. Chem. Soc.* **2005**, *127*, 3090–3099.

[5] a) S. M. Holmes, G. S. Girolami, *J. Am. Chem. Soc.* **1999**, *121*, 5593–5594; b) T. Kashiwagi, S.-i. Ohkoshi, H. Seino, Y. Mizobe, K. Hashimoto, *J. Am. Chem. Soc.* **2004**, *126*, 5024–5025; c) M. Verdaguer, *Coord. Chem. Rev.* **1999**, *190–192*, 1023–1047; d) H.-Z. Kou, S. Gao, J. Zhang, G.-H. Wen, G. Su, R. K. Zheng, X. X. Zhang, *J. Am. Chem. Soc.* **2001**, *123*, 11809–11810.

[6] a) A. Dei, *Angew. Chem. Int. Ed.* **2005**, *44*, 1160–1163; b) Y. Arimoto, S.-i. Ohkoshi, Z. J. Zhong, H. Seino, Y. Mizobe, K. Hashimoto, *J. Am. Chem. Soc.* **2003**, *125*, 9240–9241; c) J. M. Herrera, V. Marvaud, M. Verdaguer, J. Marrot, M. Kalisz, C. Mathonière, *Angew. Chem. Int. Ed.* **2004**, *43*, 5468–5471; d) S.-i. Ohkoshi, H. Tokoro, T. Z, Y. Hozumi, K. Hashimoto, C. Mathonière, I. Bord, G. Rombaut, M. Verlelst, C. C. d. Moulin, F. Villain, *J. Am. Chem. Soc.* **2006**, *128*, 270–277; e) S.-i. Ohkoshi, S. Ikeda, T. Hozumi, T. Kashiwagi, K. Hashimoto, *J. Am. Chem. Soc.* **2006**, *128*, 5320–5321.

[7] a) K. Inoue, K. Kikuchi, M. Ohba, H. Okawa, *Angew. Chem. Int. Ed.* **2003**, *42*, 4810–4813; b) W. Kenaeko, S. Kitagawa, M. Ohba, *J. Am. Chem. Soc.* **2007**, *129*, 248–249.

[8] a) R. Podgajny, C. Deaplanches, B. Sieklucka, R. Sessoli, V. Villar, C. Paulsen, W. Wernsdorfer, Y. Dromzée, M. Verdaguer, *Inorg. Chem.* **2002**, *41*, 1323–1327; b) F. Bonadio, M. Gross, H. Stoeckli-Evans, S. Decurtins, *Inorg. Chem.* **2002**, *41*, 5891–5896; c) D. E. Freedman, M. V. Bennett, J. R. Long, *Dalton Trans.* **2006**, 2829–2834; d) Z. J. Zhong, H. Seino, Y. Mizobe, M. Hidai, A. Fujishima, S.-i. Ohkoshi, K. Hashimoto, *J. Am. Chem. Soc.* **2000**, *122*, 2952–2953; e) Y. Song, P. Zhang, X.-M. Ren, X.-F. Shen, Y.-Z. Li, X.-Z. You, *J. Am. Chem. Soc.* **2005**, *127*, 3708–3709; f) J. H. Lim, J. H. Yoon, H. C. Kim, C. S. Hong, *Angew. Chem. Int. Ed.* **2006**, *45*, 7424–7426; g) J. H. Lim, H. S. Yoo, J. H. Yoon, E. K. Koh, H. C. Kim, C. S. Hong, *Polyhedron* **2008**, *27*, 299–303.

[9] a) R. Lescouëzec, L. M. Toma, J. Vaissermann, M. Verdaguer, F. S. Delgado, C. Ruiz-Pérez, F. Lloret, M. Julve, *Coord. Chem. Rev.* **2005**, *249*, 2691–2729; b) Y.-Z. Zhang, S. Gao, Z.-M. Wang, G. Su, H.-L. Sun, F. Pan, *Inorg. Chem.* **2005**, *44*, 4534–4545.

[10] W.-W. Ni, Z.-H. Ni, A.-L. Cui, X. Liang, H.-Z. Kou, *Inorg. Chem.* **2007**, *46*, 22–33.

[11] a) L. M. Toma, R. Lescouëzec, F. Lloret, M. Julve, J. Vaissermann, M. Verdaguer, *Chem. Commun.* **2003**, 1850–1851; b) R. Lescouëzec, J. Vaissermann, C. Ruiz-Pérez, F. Lloret, R. Carrasco, M. Julve, M. Verdaguer, Y. Dromzee, D. Gatteschi, W. Wernsdorfer, *Angew. Chem. Int. Ed.* **2003**, *42*, 1483–1486; c) L. M. Toma, R. Lescouëzec, J. Pasán, C. Ruiz-Pérez, J. Vaissermann, J. Cano, R. Carrasco, W. Wernsdorfer, F. Lloret, M. Julve, *J. Am. Chem. Soc.* **2006**, *128*, 4842–4853.

[12] a) W. Liu, C.-F. Wang, Y.-Z. Li, J.-L. Zuo, X.-Z. You, *Inorg. Chem.* **2006**, *45*, 10058–10065; b) H.-R. Wen, C.-F. Wang, Y. Song, S. Gao, J.-L. Zuo, X.-Z. You, *Inorg. Chem.* **2006**, *45*, 8942–8949; c) Z.-G. Gu, Q.-F. Yang, W. Liu, Y. Song, T.-Z. Li, J.-L. Zuo, X.-Z. You, *Inorg. Chem.* **2006**, *45*, 8895–8901; d) S. Wang, J.-L. Zuo, H.-C. Zhou, H. J. Choi, Y. Ke, J. R. Long, X.-Z. You, *Angew. Chem. Int. Ed.* **2004**, *43*, 5940–5943; e) D. Li, S. Parkin, G. Wang, G. T. Yee, A. V. Prosvirin, S. M. Holmes, *Inorg. Chem.* **2005**, *44*, 4903–4905; f) D. Li, S. Parkin, G. Wang, G. T. Yee, R. Clérac, W. Wernsdorfer, S. M. Holmes, *J. Am. Chem. Soc.* **2006**, *128*, 4214–4215; g) J. Y. Yang, M. P. Shores, J. J. Sokol, J. R. Long, *Inorg. Chem.* **2003**, *42*, 1403–1419; h) S. Wang, J.-L. Zuo, S. Gao, Y. Song, H.-C. Zhuo, Y.-Z. Zhang, X.-Z. You, *J. Am. Chem. Soc.* **2004**, *126*, 8900–8901.

[13] a) R. Lescouëzec, J. Vaissermann, L. M. Toma, R. Carrasco, F. Lloret, M. Julve, *Inorg. Chem.* **2004**, *43*, 2234–2236; b) Z.-H. Ni, H.-Z. Kou, L.-F. Zhang, W.-W. Ni, Y.-B. Jiang, A.-L. Cui, J. Ribas, O. Sato, *Inorg. Chem.* **2005**, *44*, 9631–9633; c) J. I. Kim, H. S. Yoo, E. W. Koh, H. C. Kim, C. S. Hong, *Inorg. Chem.* **2007**, *46*, 8481–8483; d) J. I. Kim, H. S. Yoo, E. W. Koh, C. S. Hong, *Inorg. Chem.* **2007**, *46*, 10461–10463.

[14] a) Z.-H. Ni, H.-Z. Kou, Y.-H. Zhao, L. Zheng, R.-J. Wang, A.-L. Cui, O. Sato, *Inorg. Chem.* **2005**, *44*, 2050–2059; b) Z.-H. Ni, H.-Z. Kou, L. Zheng, Y.-H. Zhao, L.-F. Zhang, R.-J. Wang, A.-L. Cui, O. Sato, *Inorg. Chem.* **2005**, *44*, 4728–4736.

[15] a) J. J. Sokol, A. G. Hee, J. R. Long, *J. Am. Chem. Soc.* **2002**, *124*, 7656–7657; b) E. J. Schelter, A. V. Prosvirin, K. R. Dunbar, *J. Am. Chem. Soc.* **2004**, *126*, 15004–15005; c) J. H. Yoon, H. C. Kim, C. S. Hong, *Inorg. Chem.* **2005**, *44*, 7714–7716; d) J. H. Yoon, J. H. Lim, H. C. Kim, C. S. Hong, *Inorg. Chem.* **2006**, *45*, 9613–9615; e) J. H. Yoon, J. H. Lim, S. W. Choi, H. C. Kim, C. S. Hong, *Inorg. Chem.* **2007**, *46*, 1529–1531.

[16] O. Kahn, *Molecular Magnetism*, VCH, Weinheim, **1993**.

[17] a) J. H. Lim, Y. S. You, H. S. Yoo, J. H. Yoon, J. I. Kim, E. K. Koh, C. S. Hong, *Inorg. Chem.* **2007**, *46*, 10578–10586; b) J. H. Lim, J. S. Kang, H. C. Kim, E. K. Koh, C. S. Hong, *Inorg. Chem.* **2006**, *45*, 7821–7827.

[18] K. R. Dunbar, R. A. Heintz, *Prog. Inorg. Chem.* **1997**, *45*, 283–391.

[19] M. Llunell, D. Casanova, J. Cirera, J. M. Bofill, P. Alemany, S. Alvarez, M. Pinsky, D. Avnir, *SHAPE*, v1.1b, Barcelona, **2005**.

[20] a) D. Visinescu, C. Desplanches, I. Imaz, V. Bahers, R. Pradhan, F. A. Villamena, P. Guionneau, J.-P. Sutter, *J. Am. Chem. Soc.* **2006**, *128*, 10202–10212; b) T. S. Venkatakrishnan, R. Rajamani, S. Ramasesha, J.-P. Sutter, *Inorg. Chem.* **2007**, *46*, 9569–9574.

[21] R. Lescouëzec, F. Lloret, M. Julve, J. Vaissermann, M. Verdaguer, *Inorg. Chem.* **2002**, *41*, 818–826.

[22] H. Zhao, M. Shatruk, A. V. Prosvirin, K. R. Dunbar, *Chem. Eur. J.* **2007**, *13*, 6573–6589.

[23] Z. J. Zhong, H. Seino, Y. Mizobe, M. Hidai, V. Verdaguer, S.-i. Ohkoshi, K. Hashimoto, *Inorg. Chem.* **2000**, *39*, 5095–5101.

[24] J. Szklarzewicz, *Inorg. Chim. Acta* **1993**, *205*, 85–89.

[25] S. McCann, M. McCann, R. M. T. Casey, M. Jackman, M. Devereux, V. McKee, *Inorg. Chim. Acta* **1998**, *279*, 24–29.

[26] G. M. Sheldrick, *SADABS, A program for area detector absorption corrections*, University of Göttingen, Germany, **1994**.

[27] G. M. Sheldrick, *SHELXTL*, version 5, Bruker AXS, Madison, Wisconsin, **1995**.

Received: March 5, 2008
Published Online: May 6, 2008

